Direct Observation of Hydrogen Atom Adducts to Nitromethane and Methyl Nitrite. A Variable-Time Neutralization−Reionization Mass Spectrometric and ab Initio/RRKM Study

Miroslav Polášek and František Tureček*

Department of Chemistry, Bagley Hall, Box 351700, University of Washington, Seattle, Washington 98195-1700

Received: June 16, 1999; In Final Form: September 16, 1999

Variable-time neutralization−reionization mass spectrometry was used to generate elusive radicals $CH_3NO_2H^•$ (**1**), $CH_3O(H)-NO^•$ (**2**) $CH_3O-N(H)-O^•$ (**3**), and $CH_3O-N-OH^•$ (**4**) that represent hydrogen atom adducts to nitromethane and methyl nitrite, respectively. Radicals **1**, **3**, and **4** were stable species on the 3.7 μs time scale of the experiment. Radical **2** dissociated completely to CH_3OH and NO. The major unimolecular dissociations of **1** formed $CH_3NO + OH^•$ and $CH_3^• + NO_2H$, whereas loss of $H^•$ to form CH_3NO_2 was insignificant. Gaussian 2(MP2) and density functional theory calculations provided the structures and bond dissociation energies of **1**−**4**. The relevant parts of the potential-energy surface were used for RRKM and transition-state theory calculations of unimolecular dissociation kinetics. The calculated branching ratios for **1** were in accord with experiment. The unimolecular chemistry of radicals **1**−**4** formed by femtosecond collisional electron transfer can be accounted for by the properties of the ground electronic states of **1**−**4**.

Introduction

The complex chemistry of flames involves a multitude of radical and ion intermediates that have been extensively studied.[1] In particular, nitromethane served as a model for hydrogen atom trapping in flames, and the bimolecular kinetics of the $CH_3NO_2 + H^•$ reaction has been investigated by several groups.[2] A radical intermediate, $CH_3NO_2H^•$ (**1**), has been postulated to play a role in the formation of reaction products, $CH_3^• + NO_2H$ and $CH_3NO + OH^•$.[3] However, intermediate **1** has never been detected and the thermochemistry of its dissociations is unknown.[4]

We now report the first generation and detection of isolated **1** in the gas phase. We use neutralization−reionization mass spectrometry[5] to generate the radical by femtosecond electron transfer to a stable cation $CH_3NO_2H^+$ ($\mathbf{1}^+$). The kinetics of purely unimolecular dissociations of **1** is investigated by variable-time measurements.[6] Formation of excited electronic states of **1** is probed by laser photoexcitation.[7] We also report the generation of elusive radicals derived from methyl nitrite, $CH_3O(H)-NO^•$ (**2**), $CH_3O-N(H)-O^•$ (**3**), and $CH_3O-N-OH^•$ (**4**). Gaussian 2 (MP2) ab initio[8] and density functional theory calculations are used to provide relative energies of the radicals and ions under study. Unimolecular kinetics of radical dissociations is treated by Rice−Ramsperger−Kassel−Marcus (RRKM) theory[9] using the G2(MP2) potential energy surface.

Experimental Section

Methods. Measurements were carried out on a tandem quadrupole acceleration−deceleration mass spectrometer described previously.[10] Precursor ions were generated in a tight chemical ionization source. Typical ionization conditions were as follows: electron energy 100 eV, emission current 1−2 mA, temperature 280−300 °C, ion source potential 80 V. CH_4, CD_4, CH_3OH, CH_3OD, CD_3OH, CD_3OD, and H_2O were used as reagent gases at pressures $1.0-1.5 \times 10^{-4}$ Torr as read on an ionization gauge located at the diffusion pump intake. Electron ionization (EI) was used to generate cation radicals $CH_3NO_2^{+•}$, NO_2^+, $CH_3OH^{+•}$ $CH_3OD^{+•}$, $CD_3OH^{+•}$, and $CD_3OD^{+•}$. Typical EI conditions were as follows: electron energy 70 eV, source temperature 280−300 °C, and sample pressure $5-8 \times 10^{-6}$ Torr. Stable precursor ions were passed through a quadrupole mass filter operated in the radio frequency-only mode, accelerated to the total kinetic energy of 8250 eV, and neutralized in the collision cell floated at −8170 V. The precursor ion lifetimes were 30−40 μs. Dimethyl disulfide (DMDS) was admitted to the differentially pumped collision cell at a pressure such as to achieve 70% transmittance of the precursor ion beam. The ions and neutrals were allowed to drift to a four segment conduit,[6] where the ions were reflected by the first segment floated at +250 V. The fast neutral species were reionized in the second collision cell by collision with oxygen at a pressure adjusted such as to achieve 70% transmittance of the precursor ion beam. The ions formed in the second collision cell were decelerated, energy filtered, and analyzed by a quadrupole mass filter operated at unit mass resolution. The instrument was tuned daily to maximize the ion current of reionized $CS_2^{+•}$. Typically, 30 repetitive scans were accumulated per spectrum, and each spectrum was reproduced at least three times over a period of several weeks. Variable-time measurements were carried out as described previously.[6]

Collisionally activated dissociation (CAD) spectra were measured on a JEOL HX-110 double-focusing mass spectrometer of forward geometry (the electrostatic sector E precedes the magnet B). Collisions with air were monitored in the first field-free region at pressure to achieve 70% transmittance of the ion beam at 10 keV. The spectra were obtained by scanning E and B simultaneously while maintaining a constant B/E ratio (B/E linked scan).

Materials. Methane (Matheson, 99.97%), CD_4 (Cambridge Isotope Laboratories, 99% D), methanol (Aldrich), CD_3OH (Aldrich, 99% D), CH_3OD (Cambridge Isotope Laboratories, 99% D), CD_3OD (Cambridge Isotope Laboratories, 99.8% D), dimethyl disulfide (DMDS, Aldrich), nitromethane (Aldrich,

10.1021/jp991984l CCC: $18.00
Published on Web 11/03/1999

99%) and CD_3NO_2 (Aldrich, 99% D) were used as received. Methyl nitrites CH_3ONO and CD_3ONO were synthesized according to a literature procedure[11] by dropwise addition of 20% sulfuric acid to a stoichiometric mixture of appropriate methanol and sodium nitrite. The escaping gas was washed by a solution of sodium hydroxide and dried by passing through a tube containing anhydrous calcium chloride. Trap-to-trap distillation was used before the product was stored in the dark at −38 °C. The purity was verified by mass spectrometry.

Calculations

Standard ab initio and density functional theory calculations were performed using the Gaussian 94 suite of programs.[12] Geometries were optimized using Becke's hybrid functional (B3LYP)[13] and the 6-31+G(d,p) or 6-311+G(3df,2p) basis sets. For selected species and dissociation pathways, geometries were also optimized with perturbational Møller−Plesset theory,[14] MP2(FULL)/6-31+G(d,p).[15] Basis sets of this quality have been shown previously to give mostly reliable equilibrium geometries for neutral molecules and ions.[16] Spin-unrestricted calculations (UB3LYP or UMP2) were used for open-shell systems. Spin contamination in UMP2 calculations was substantial for $[C,H_4,N,O_2]$ radicals and transition states and it was partially corrected using Schlegel's projection method.[17] The optimized structures were characterized by harmonic frequency analysis as local minima (all frequencies real) or first-order saddle points (one imaginary frequency). The B3LYP/6-31+G(d,p) frequencies were scaled by 0.961 (ref 18, for other scaling factors see ref 19) and used to calculate zero-point vibrational energies (ZPVE) and enthalpy corrections. The UMP2(FULL)/6-31+G(d,p) frequencies were scaled by 0.931 which provided the best match for ZPVE calculated by B3LYP and MP2(FULL). Single-point energies were calculated at the Gaussian-2(MP2) level of theory.[8] This consisted of MP2/6-311+G(3df,2p), MP2/6-311G(d,p), and QCISD(T)/6-311G(d,p)[20] calculations which were combined to provide effective QCISD(T)/6-311+G(3df,2p) energies which were corrected for the ZPVE and the number of valence electrons.[8] Note that most relative energies calculated in this work refer to isoelectronic systems in which the empirical corrections cancel out. The calculated total energies are available as Supporting Information.

The G2(MP2) total energies were much less sensitive to spin contamination; the G2(PMP2) and G2(UMP2) energies were all within 0.7 mhartree (1.8 kJ mol^{-1}). The only exception was the G2(MP2) energy of $CH_3NO_2^{+\bullet}$ when based on a B3LYP/6-31+G(d,p) optimized geometry that was encumbered by very large spin contamination which could not be corrected by spin projection (see Supporting Information). However, G2(UMP2) and G2(PMP2) single-point energies based on a MP2(FULL)/6-31+G(d,p) optimized geometry were within 0.5 mhartree and provided an accurate ionization energy for nitromethane and an acceptable dissociation energy for the cation radical.

Franck−Condon energies in vertical neutralization and reionization were taken as absolute differences between the total B3LYP/6-311+G(3df,2p) energies of fully optimized ion or neutral structures and those in which an electron has been added to an optimized cation structure or subtracted from an optimized neutral structure. No zero-point corrections were applied to the calculated Franck−Condon energies.

RRKM calculations used Hase's program[21] that was recompiled for MS-DOS and run under Windows NT.[16c] Vibrational state densities were obtained by direct count of quantum states in 2 kJ mol^{-1} steps for internal energies up to 80−120 kJ mol^{-1} above the threshold. The rotational states were treated adiabatically[22] and the microscopic rate constants *k(E,J,K)* were Boltzmann-averaged over the thermal distribution of rotational J and K states pertaining to the ion source temperature. Thermal rate constants were calculated using the standard transition state theory formulas.[23] The activation energies were taken from G2(PMP2) calculations, the partition functions were calculated from the B3LYP/6-31+G(d,p) moments of inertia and scaled harmonic frequencies.

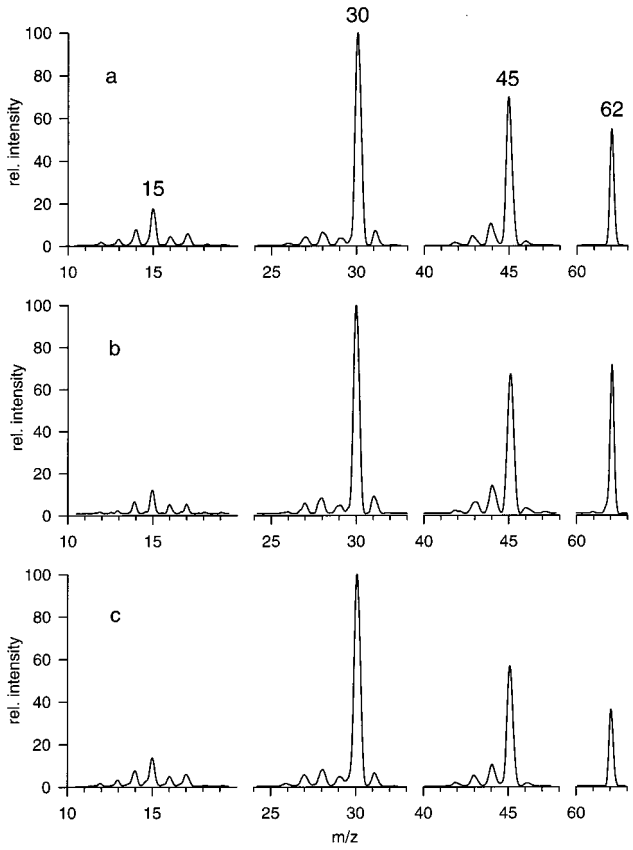

Figure 1. Neutralization (CH_3SSCH_3, 70% transmittance)-reionization (O_2, 70% transmittance) mass spectra of (a, top) $\mathbf{1}^+$ by protonation with CH_5^+, (b, middle) **1** by protonation with H_3O^+. (c, bottom): Neutralization (CH_3SSCH_3, 70% transmittance)−collisional activation (He, 50% transmittance)−reionization (O_2, 70% transmittance) mass spectrum of $\mathbf{1}^+$ by protonation with CH_5^+. The *m/z* regions not shown in the spectra contained no peaks.

Results and Discussion

Formation and Dissociations of $CH_3NO_2H^+$ and $CH_3NO_2H^\bullet$. The precursor cation $\mathbf{1}^+$ was generated by exothermic protonation of nitromethane under conditions of chemical ionization. From the proton affinity of CH_3NO_2, PA = 755 kJ mol^{-1},[24] protonations with CH_5^+ ($PA(CH_4)$ = 544 kJ mol^{-1})[24] and H_3O^+ ($PA(H_2O)$ = 691 kJ mol^{-1})[24] were 211 kJ mol^{-1} and 64 kJ mol^{-1} exothermic, respectively. Collisional neutralization of $\mathbf{1}^+$ was performed with dimethyl disulfide (DMDS, IE_v = 8.96 eV[24]) as an electron donor. From the calculated vertical recombination energy of $\mathbf{1}^+$ (7.3 eV, vide infra) vertical electron transfer from DMDS was ∼1.7 eV endoergic.

The NR mass spectrum of $\mathbf{1}^+$ produced by protonation of nitromethane by CH_5^+ showed an abundant survivor ion at *m/z* 62 corresponding to 11% of the sum of NR ion intensities (% ΣI_{NR}) (Figure 1a). Less exothermic protonation with H_3O^+ resulted in an increased relative abundance of survivor $\mathbf{1}^+$ ([**1**], 17% ΣI_{NR}, Figure 1b). Similar effects of precursor ion internal energy have been observed previously.[25] The primary fragments

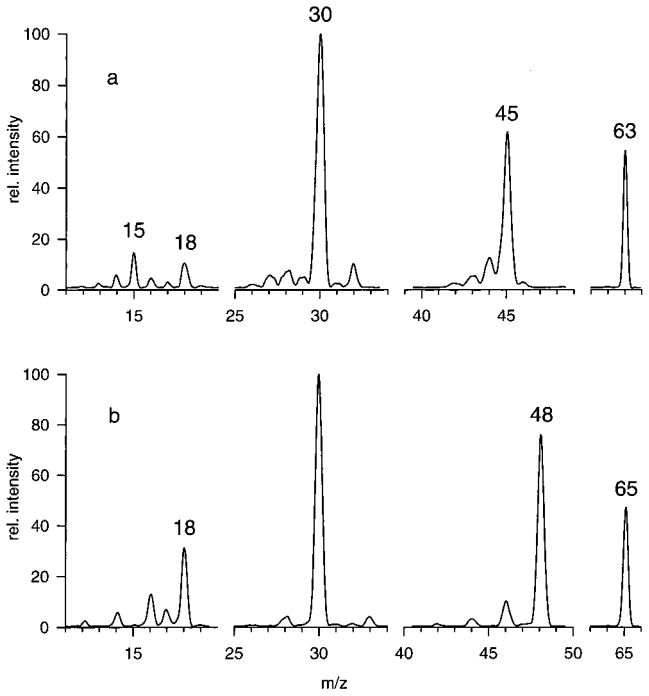

Figure 2. Neutralization (CH_3SSCH_3, 70% transmittance)-reionization (O_2, 70% transmittance) mass spectra of (a, top) $CH_3NO_2D^+$ and (b, bottom) $CD_3NO_2H^+$. The *m*/*z* regions not shown in the spectra contained no peaks.

in the NR mass spectra were $CH_3NO^{+\bullet}$ (*m*/*z* 45, 23% ΣI_{NR}), OH^+ (*m*/*z* 17, 2% ΣI_{NR}) and CH_3^+ (*m*/*z* 15, 6% ΣI_{NR}). The $NO_2H^{+\bullet}$ ion (*m*/*z* 47) that was complementary to CH_3^+ was not detected. NO^+ (*m*/*z* 30) was the most abundant ion in the NR mass spectra (36 and 34% ΣI_{NR}, respectively, Figure 1a,b). Collisional activation with helium at 70%, 50%, and 30% transmittance of intermediate **1** resulted in a sequential decrease of [**1**] and $[CH_3NO]^{+\bullet}$ while the relative abundances of NO^+ and OH^+ increased (Figure 1c).

The NR spectra of deuterated ions $CH_3NO_2D^+$ ($\mathbf{1a}^+$) and $CD_3NO_2H^+$ ($\mathbf{1b}^+$) showed dissociations similar to those of $\mathbf{1}^+$ (Figure 2a,b). In particular, the label remained confined in the original functional group, e.g., OD^+ from $\mathbf{1a}^+$ and CD_3^+ from $\mathbf{1b}^+$. No hydrogen exchange between the OH and CH_3 groups was observed upon NR.

To identify consecutive neutral and ion dissociations following NR, we obtained reference collisionally activated dissociation (CAD) spectra of $\mathbf{1}^+$ and NR mass spectra of the presumed or observed primary dissociation products of **1**. CAD of $\mathbf{1}^+$ produced, in the order of decreasing abundance, NO^+ (loss of CH_3OH, 45% ΣI_{CAD}), $CH_3NO^{+\bullet}$ (loss of $OH^\bullet$, 28% ΣI_{CAD}), CH_2NO^+ (loss of H_2O, 12% ΣI_{CAD}), NO_2^+ (loss of CH_4, 4.4% ΣI_{CAD}), and $CHNO^{+\bullet}$ (loss of $H_2O + H$, 4% ΣI_{CAD}). Note that the complementary stable neutral fragments from CAD (methanol and water) did not give rise to appreciable peaks in the NR spectrum of $\mathbf{1}^+$ (Figure 1). This strongly indicated that collisional electron transfer from DMDS was not accompanied by appreciable CAD.

NR of $CH_3NO^{+\bullet}$ provided a moderately strong survivor ion at *m*/*z* 45 and major fragments due to formation of NO^+ and CH_3^+. These were due to a combination of neutral and post-reionization dissociations of CH_3NO, as reported previously.[26]

NR of $NO_2H^{+\bullet}$ was measured for an ion prepared by protonation of NO_2 with CH_5^+. According to the calculated topical proton affinities in NO_2 (vide infra), protonation with CH_5^+ can occur exothermically only at one of the oxygen atoms

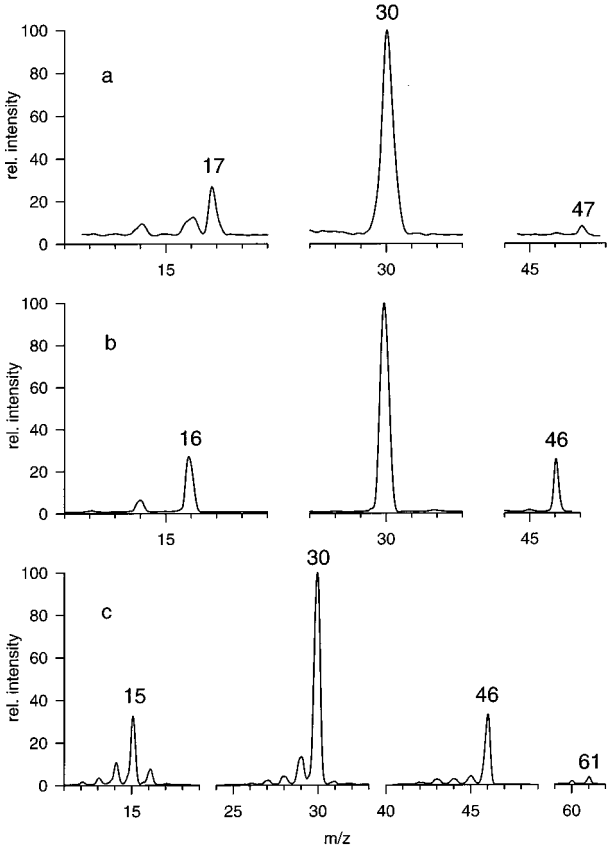

Figure 3. Neutralization (CH_3SSCH_3, 70% transmittance)−reionization (O_2, 70% transmittance) mass spectra of (a, top) $HONO^{+\bullet}$ by protonation of NO_2, (b, middle) NO_2^+, and (c, bottom) $CH_3NO_2^{+\bullet}$. The *m*/*z* regions not shown in the spectra contained no peaks.

to give the cation-radical of nitrous acid, $HONO^{+\bullet}$. NR of $HONO^{+\bullet}$ yielded a very weak survivor ion at *m*/*z* 47 and major fragments NO^+ and OH^+ (Figure 3a). This indicated that HONO formed by dissociation of **1** would be difficult to detect because of lack of signature peaks in the spectrum. Preparation of $HONO^{+\bullet}$ by electron ionization of stable neutral HONO[27] was not attempted because of large predicted Franck−Condon effects (vide infra).

NR of NO_2^+ gave a stable survivor ion at *m*/*z* 46 in addition to NO^+, O^+, and N^+ (Figure 3b). Finally, NR of the nitromethane cation-radical ($\mathbf{5}^{+\bullet}$) yielded a weak but detectable survivor ion at *m*/*z* 61 and fragments NO_2^+ (*m*/*z* 46), $CH_3NO^{+\bullet}$ (*m*/*z* 45), NO^+, CHO^+, $CO^{+\bullet}$, O^+, CH_3^+, etc. (Figure 3c), in agreement with the Xe/O_2 NR spectrum reported previously by Egsgaard et al.[28]

Variable-Time Measurements. Dissociations of neutral **1** and reionized $\mathbf{1}^+$ were distinguished by variable-time NR spectra.[6] The time-dependent relative intensities of reionized $\mathbf{1}^+$, $CH_3NO^{+\bullet}$, OH^+, and CH_3^+ were fitted into kinetic equations to yield unimolecular rate parameters for neutral and ion dissociations.[6] Least-squares fits were obtained for bimodal exponential decay in the neutral channel including one fast ($k_N > 10^7\ s^{-1}$) and one slow ($k_N = 10^4-10^6\ s^{-1}$) dissociation and a single-exponential decay (k_i) in the ion channel. Solving the equations required estimates of the reionization cross sections (σ) for CH_3NO, $OH^\bullet$ and $CH_3^\bullet$ relative to that of **1**. These were obtained from the Fitch−Sauter atomic increment scheme[29] assuming that collisional reionization followed rules similar to those governing electron ionization. From the atomic increments for C, H, N, and O, we calculated $\sigma(CH_3NO)/\sigma(\mathbf{1}) = 0.779$, $\sigma(OH)/\sigma(\mathbf{1}) = 0.348$ and $\sigma(CH_3)/\sigma(\mathbf{1}) = 0.567$.

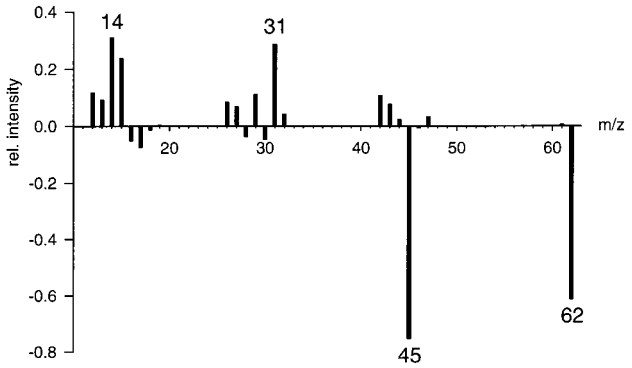

Figure 4. Difference NR spectra from photoexcitation of **1** at 488 and 514.5 nm.

The formation of CH_3NO and $OH^\bullet$ showed predominant contribution from neutral dissociations, e.g., $k_N(CH_3NO) = (4.8 \pm 0.3) \times 10^5\ s^{-1}$ and $k_N(OH^\bullet) = (5.4 \pm 0.9) \times 10^5\ s^{-1}$, from three measurements. The rate parameters correlated for both observation channels, which provided unequivocal evidence for a dissociation originating from the same neutral precursor.[30] The rate parameters for ion dissociation in reionized $\mathbf{1}^+$ were smaller, e.g., $k_i(CH_3NO^{+\bullet}) = (2.5 \pm 1.1) \times 10^5\ s^{-1}$, $k_i(OH^+) = (-0.1 \pm 0.6) \times 10^5\ s^{-1}$, and the values did not correlate because of different ionization energies of the products.[24] Best fits for k_N were obtained for single-exponential kinetic model, which indicated that the dissociation of **1** occurred on a μs time scale. For the C−N bond rupture in **1** producing $CH_3^\bullet$ and HONO, only one observation channel was available because of the lack of $HONO^{+\bullet}$ peak in the spectrum (vide supra). The corresponding rate parameters were obtained as $k_N(CH_3^\bullet) = (5.3 \pm 0.9) \times 10^5\ s^{-1}$ and $k_i(CH_3^+) = (0.1 \pm 0.2) \times 10^5\ s^{-1}$ that favored the neutral dissociation.

Photoexcitation of $CH_3NO_2H^\bullet$. Irradiation of the neutral and reionized ion beam with the combined 488 nm (2.54 eV) and 514.5 nm (2.41 eV) lines from the Ar-ion laser resulted in small changes of the relative intensities of several ions (Figure 4). In particular, $\mathbf{1}^+$ decreased from 9.0 ± 0.1% to 8.4 ± 0.3% ΣI_{NR}, and $CH_3NO^{+\bullet}$ decreased from 19.7 ± 0.4% to 18.9 ± 0.6% ΣI_{NR} as a result of interaction with the laser light. The changes in relative intensities of the other ion species were within the reproducibility limits. The laser-induced depletion of $\mathbf{1}^+$ and $CH_3NO^{+\bullet}$ can be due to photofragmentation of either neutral intermediates or ions, or combination thereof.

Formation and Dissociations of $CH_3O(H)-NO^+$ and $CH_3O(H)-NO^\bullet$. The precursor cation $\mathbf{2}^+$ was generated by chemical ionization of methyl nitrite with $CH_3OH_2^+/CH_3OH$. Under CI conditions a sequence of ion−molecule reactions took place. Self-protonation of methanol (eq 1) was followed by proton transfer to methyl nitrite (eq 2). According to calculations

$$CH_3OH^{+\bullet} + CH_3OH \rightarrow CH_3OH_2^+ + CH_2OH^\bullet \quad (1)$$

$$CH_3O-NO + CH_3OH_2^+ \rightarrow CH_3O(H)-NO^+ + CH_3OH \quad (2)$$

(vide infra), the proton affinity of methyl nitrite, PA = 799 kJ mol^{-1},[24] favors protonation at the inner oxygen atom. The topical proton affinities of the nitrogen atom and terminal oxygen were calculated as 703 and 698 kJ mol^{-1}, respectively (vide infra)). Thus, $CH_3OH_2^+$ (PA = 754 kJ mol^{-1})[24] can protonate methyl nitrite exothermically only at the inner oxygen to produce stable cation $\mathbf{2}^+$. However, ion $\mathbf{2}^+$ further reacted with neutral methanol which was the most abundant species in the ion source. This hidden reaction was made obvious by deuterium labeling. For example, $CD_3O(H)-NO^+$ formed by proton transfer from $CH_3OH_2^+$ to CD_3ONO according to eq 2 further reacted with CH_3OH by NO^+ transfer to produce almost exclusively $CH_3O(H)NO^+$ (eq 3).

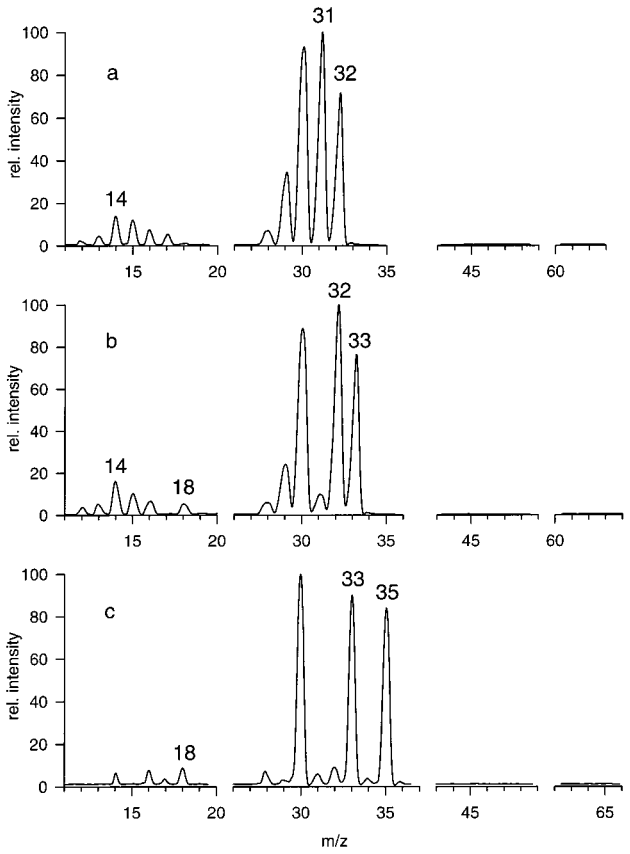

Figure 5. Neutralization (CH_3SSCH_3, 70% transmittance)−reionization (O_2, 70% transmittance) mass spectra of (a, top) $\mathbf{2}^+$, (b, middle) $CH_3O(D)-NO^+$, and (c, bottom) $CD_3O(H)-NO^+$. The *m*/*z* regions not shown in the spectra contained no peaks.

$$CD_3O(H)-NO^+ + CH_3OH \rightarrow CH_3O(H)-NO^+ + CD_3OH \quad (3)$$

Hence, deuterium labeled cations $CH_3O(D)-NO^+$ ($\mathbf{2a}^+$), $CD_3O(H)-NO^+$ ($\mathbf{2b}^+$), and $CD_3O(D)-NO^+$ ($\mathbf{2c}^+$) were prepared from CH_3ONO according to reactions 1−3 using CH_3OD, CD_3OH, and CD_3OD, respectively.

The NR mass spectrum of $\mathbf{2}^+$ showed no survivor ion. The dominant species were methanol that, following collisional ionization, was characterized by ions at *m*/*z* 32, 31, 29, and NO which gave the ion at *m*/*z* 30 (Figure 5a). Since $CH_3OH^{+\bullet}$ dissociates to form $CH_2O^{+\bullet}$ at *m*/*z* 30 which was not resolved from NO^+, the contributions of methanol fragments and NO^+ were deconvoluted through mass shifts in the spectra of $\mathbf{2a}^+$ and $\mathbf{2b}^+$ (Figure 5b,c). We also obtained reference NR mass spectra of CH_3OD and CD_3OH. Interestingly, methanol cation-radicals formed by dissociation of neutral **2**, **2a**, **2b**, and **2c** followed by reionization showed remarkably less dissociation due to the loss of H or D than did those sampled directly for NR.[25a] For methanol cation-radicals prepared by electron ionization, the ratios in the corresponding NR spectra were $[CH_3OH]^{+\bullet}/[CH_2OH]^+ = 0.39$, $[CD_3OH]^{+\bullet}/[CD_2OH]^+ = 0.36$, $[CH_3OD]^{+\bullet}/[CH_2OD]^+ = 0.44$, and $[CD_3OD]^{+\bullet}/[CD_2OD]^+ = 0.43$. In contrast, when CH_3OH, CH_3OD, and CD_3OH were generated by NR of $\mathbf{2}^+$, $\mathbf{2a}^+$, $\mathbf{2b}^+$, and $\mathbf{2c}^+$, respectively, the corresponding

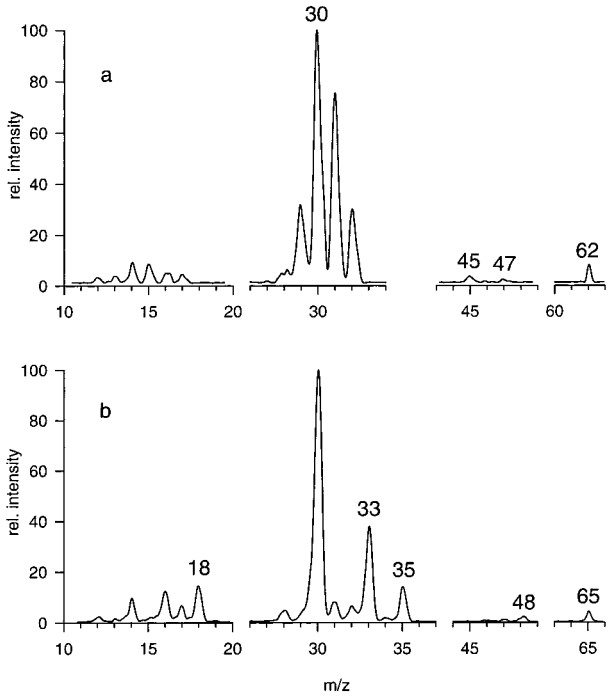

Figure 6. Neutralization (CH_3SSCH_3, 70% transmittance)-reionization (O_2, 70% transmittance) mass spectra of (a, top) $\mathbf{3}^+ + \mathbf{4}^+$ by protonation with CH_5^+, (b, bottom) $CD_3O{-}NH{=}O^+ + CD_3O{-}N{-}OH^+$ by protonation of CD_3ONO with CH_5^+. The *m*/*z* regions not shown in the spectra contained no peaks.

ratios were 0.65, 0.69, 1.04 and 0.98, respectively. This showed that methanol molecules formed by NR of $\mathbf{2}^+$, $\mathbf{2a}^+$, $\mathbf{2b}^+$, and $\mathbf{2c}^+$ had somewhat lower internal energies than those formed by collisional neutralization of methanol cation-radicals.[25a] It should be noted that with $\mathbf{2a}^+$, $\mathbf{2b}^+$ and $\mathbf{2c}^+$, the relative abundances of fragment ions were affected by isotope effects. Despite some peak overlaps at *m*/*z* 30 (NO^+, $CH_2O^{+\bullet}$, and CDO^+), and *m*/*z* 14 (N^+, $CH_2^{+\bullet}$, and CD^+), the NO/methanol ratios were estimated from the sums of ion intensities as 0.41, 0.42, 0.44, and 0.41 for $CH_3O(H){-}NO^+$, $CD_3O(H){-}NO^+$, $CH_3O(D){-}NO^+$ and $CD_3O(D){-}NO^+$, respectively. Considering the different ionization energies of methanol (10.85 eV) and NO (9.25 eV), the NO/methanol ratios strongly suggested that these fragments were not formed by dissociation of reionized $\mathbf{2}^+$ which would strongly prefer NO^+. By contrast, dissociation of *neutral* $CH_3O(H){-}NO^\bullet$ to CH_3OH and NO followed by reionization should yield $CH_3OH^{+\bullet}$ and NO^+ according to their ionization cross sections. The latter can be estimated from electron ionization cross sections,[31,32] as $[NO^+]/[CH_3OH^{+\bullet}] = 0.52{-}0.72$. This ratio was somewhat greater than the NO/methanol ratios measured form the NR mass spectra, indicating an additional source of methanol. This could be provided by CAD of the precursor ion $\mathbf{2}^+$ concomitant with neutralization. Comparison of the NR measured and predicted $[NO^+]/[CH_3OH^{+\bullet}]$ ratios gave an estimate for the competing collisional processes as 68% neutralization and 32% CAD. This was consistent with the fact that CAD with CH_3SSCH_3 is typically an inefficient process.

Formation and Dissociation of $CH_3O{-}N{-}OH^\bullet$ and $CH_3O{-}N(H){-}O^\bullet$. In contrast to the selective protonation of methyl nitrite with $CH_3OH_2^+$ that formed $\mathbf{2}^+$, a highly exothermic protonation of CH_5^+ was expected to form a mixture of $\mathbf{2}^+$, $\mathbf{3}^+$, and $\mathbf{4}^+$. The NR mass spectrum of CH_5^+-protonated methyl nitrite showed substantial differences from the spectrum of $\mathbf{2}^+$ (Figure 6). In particular, the NR spectrum showed a survivor ion and fragments due to loss of $CH_3^\bullet$ (*m*/*z* 47) and $OH^\bullet$ (*m*/*z* 45, Figure 6a) which were absent in the NR spectrum of $\mathbf{2}^+$. The NR spectrum of $[CD_3ONO + H^+]$ showed a survivor ion at *m*/*z* 65 and fragments due to losses of $OH^\bullet$ (*m*/*z* 48), CD_3 (*m*/*z* 47), and a small peak of NO_2^+ or CD_2NO^+ (*m*/*z* 46, Figure 6b). In addition, a peak at *m*/*z* 31 indicated formation of $[NOH]^+$ or $[NHO]^+$. The latter ions were not due to dissociation of $CD_3{-}OH^{+\bullet}$, as verified from reference NR mass spectra of $CD_3O{-}(H){-}NO^+$ and $CD_3OH^{+\bullet}$. The dissociations were compatible with isomeric precursor ions protonated at the terminal oxygen atom, $CH_3O{-}N{-}OH^+$ ($\mathbf{4}^+$) or nitrogen, $CH_3O{-}NH{=}O^+$ ($\mathbf{3}^+$), which upon collisional electron transfer gave rise to fractions of stable radicals **3** and/or **4**.

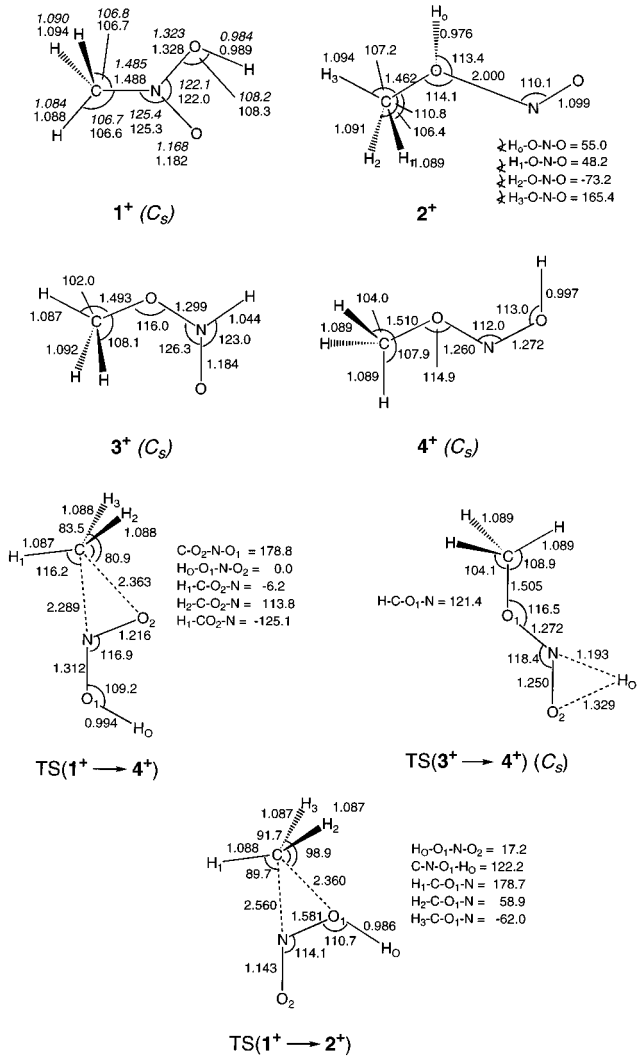

Figure 7. B3LYP/6-31+G(d,p) optimized structures of $\mathbf{1}^+$-$\mathbf{4}^+$ and transition states. Bond lengths in angstroms, bond and dihedral angles in degrees. Roman numerals: B3LYP/6-31+G(d,p) optimized structures. Italic numerals: B3LYP/6-311+G(3df,2p) optimized structures.

Ion Energies. The NR mass spectra clearly indicated that radicals **1** and **3**/**4** were stable species while **2** was not. A more quantitative insight into the cation and radical energetics was obtained by ab initio and density functional theory calculations. The B3LYP/6-31+G(d,p) optimized structures of ions $\mathbf{1}^+{-}\mathbf{4}^+$ and transition states for ion isomerizations are shown in Figure 7, the ion relative energies are given in Table 1. Structure $\mathbf{1}^+$ was unexceptional.[33] Structures $\mathbf{3}^+$, $\mathbf{4}^+$ showed long C−O bonds (Figure 7). A conspicuous feature of structure $\mathbf{2}^+$ was the very long O−N bond, so that $\mathbf{2}^+$ resembled a complex of CH_3OH with NO^+ (Figure 7).[33] From G2(MP2) calculations, $\mathbf{2}^+$ was the most stable ion isomer followed by $\mathbf{1}^+$, $\mathbf{3}^+$, and $\mathbf{4}^+$. The

TABLE 1: $[C,H_4,N,O_2]^+$ Relative Energies

	energy[a]		
species	B3LYP/6-31+G(d,p)	B3LYP/6-311+G(3df,2p)	G2(MP2)
$CH_3NO_2H^+$	0[b]	0	0
	0[c]	0	0
$CH_3O(H)-NO^+$	−20	−29	−34
	−16	−25.5	−30
$CH_3O-N(H)=O^+$	48.5	50	50
	48	50	50
$CH_3O-N=OH^+$	49	51.5	54
	49.5	52	54.5

[a] In units of kJ mol^{-1}. [b] At 0 K. [c] At 298 K.

TABLE 2: Topical Proton Affinities in Nitromethane and Methyl Nitrite

		energy[a]			
molecule	ion	B3LYP/6-31+G(d,p)	B3LYP/6-311+G(3df,2p)	G2(MP2)	exptl
CH_3NO_2	$CH_3NO_2H^+$	735[b]	739	742	
		740[c]	745	747	750[d], 755[e]
CH_3**O**NO	$CH_3O(H)NO^+$	764	780	781	
		766	782	783	797[d], 805[e]
CH_3O**N**O	$CH_3O-N(H)=O^+$	696	700	697	
		702	706	703	
CH_3ON**O**	$CH_3O-N=OH^+$	695	699	693	
		700	704	698	
N**O**$_2$	$HONO^{+\bullet}$	539	548	554	
		545	554	560	591[d], 586[e]
NO$_2$	$H-NO_2^{+\bullet}$	429	430	368	
		434	435	373	
N**O**	$NO-H^{+\bullet}$	457	460	460	
		462	465	464	
NO	$H-NO^{+\bullet}$	517	525	527	
		522	530	532	532[d]

[a] In units of kJ mol^{-1}. [b] At 0 K. [c] At 298 K. [d] Reference 35. [e] Reference 24.

topical proton affinities of nitromethane and at the nitrogen atom, methoxy, and N=O groups in methyl nitrite were calculated as 747, 703, 783, and 698 kJ mol^{-1}, respectively. The G2(MP2) and B3LYP calculated PA's for nitromethane (Table 2) were in excellent agreement with the experimental PA (750 kJ mol^{-1})[34] but showed somewhat greater deviation from the newly tabulated value (755 kJ mol^{-1}).[24] The calculations showed that the methoxy oxygen was the most basic site in methyl nitrite in agreement with the recent MP4 calculations of Aschi and Grandinetti.[33] However, both G2(MP2) and B3LYP gave proton affinities (Table 2) that were significantly lower than the experimental value (797 kJ mol^{-1}) obtained by ion-cyclotron resonance bracketing measurements.[35] The difference was even greater for the recently adjusted and tabulated value (805 kJ mol^{-1}).[24] Aschi and Grandinetti calculated PA(CH_3**O**NO) = 782 kJ mol^{-1} using the full Gaussian 2 method,[33] which was in close agreement with the present calculations but at odds with the experimental data. Mixed agreement was obtained for proton affinities of NO and NO_2 (Table 2). The calculations predicted preferential protonation on nitrogen in NO in excellent agreement with the tabulated PA value (Table 2). NO_2 was predicted to be protonated on oxygen, but the calculated PA's were substantially lower than the tabulated value. The reasons for the discrepancies in the experimental and calculated PA's are not clear. It may be noted that the cations corresponding to protonated methyl nitrite and nitrogen dioxide are weakly bound (Table 3) and prone to dissociation or ion−molecule reactions that may cause difficulties in proton affinity measurements.

Of interest to the present study were the dissociation energies of $\mathbf{1}^+$-$\mathbf{4}^+$ and the barriers to ion isomerizations. The G2(MP2) energies at 0 K are shown in a potential energy diagram (Figure 8). Loss of CH_3OH was the lowest energy dissociation of $\mathbf{2}^+$; the dissociation energy of the O−N bond in $\mathbf{2}^+$ was 97 and 99 kJ mol^{-1} at 0 and 298 K, respectively. Thus, ion $\mathbf{2}^+$ was only weakly bound against dissociation. The less stable isomers $\mathbf{1}^+$, $\mathbf{3}^+$ and $\mathbf{4}^+$ were separated by substantial barriers to hydrogen or methyl migrations (Figure 8). The lowest threshold for dissociation of $\mathbf{1}^+$ was calculated for elimination of water to form $CH_2=N=O^+$ (Figure 8). However, elimination of water was a minor dissociation of $\mathbf{1}^+$ on CAD (vide supra). Hence the reaction must be disfavored kinetically by a substantial activation barrier. Loss of methanol from $\mathbf{1}^+$ must proceed by a rate-determining isomerization to $\mathbf{2}^+$. The isomerization barrier was 200 kJ mol^{-1} above $\mathbf{1}^+$ (234 kJ mol^{-1} above $\mathbf{2}^+$ and 137 kJ mol^{-1} above the products (Figure 8). Hence, structures $\mathbf{1}^+$ and $\mathbf{2}^+$ were completely separated and could not isomerize without dissociation.[36] Large energy barriers were also obtained for isomerizations $\mathbf{1}^+ \rightarrow \mathbf{4}^+$, $\mathbf{2}^+ \rightarrow \mathbf{3}^+$, and $\mathbf{3}^+ \rightarrow \mathbf{4}^+$ (Figure 8) that separated these ion isomers. Simple dissociations of C−O and N−O bonds in $\mathbf{1}^+$, $\mathbf{3}^+$, and $\mathbf{4}^+$ were all substantially endothermic (Figure 8).

Radical Energies. Three local energy minima were found by B3LYP/6-31+G(d,p) geometry optimizations, e.g., structures **1**, **3**, and **4** (Figure 9). Radical **2** dissociated exothermically to CH_3OH and NO upon attempted geometry optimizations with B3LYP/6-31+G(d,p), UMP2(FULL)/6-31+G(d,p) and B3LYP/6-311+G(3df,2p). Hence, structure **2** is predicted to be unbound at the present level of theory. The G2(MP2) potential energy diagram for radical dissociations and isomerizations is shown in Figure 10. Radical **1** was the most stable species followed by **4** and **3**.

Dissociations by simple bond cleavages were investigated for **1**. Investigation with B3LYP/6-31+G(d,p) of the O−H bond cleavage showed a transition state (**TS1**) at d(O−H) = 1.80 Å. The G2(PMP2) potential energy barrier was E_a = 188 kJ mol^{-1} to form nitromethane and a hydrogen atom. The activation

TABLE 3: Ion Relative Stabilities and Dissociation Energies

		energy[a]			
reactant	products	B3LYP/6-31+G(d,p)	B3LYP/6-311+G(3df,2p)	G2(PMP2)	exptl[b]
$CH_3NO_2H^+$	→ $CH_3O(H)-NO^+$	−20[c]	−29	−34	
(**1**$^+$)		−16[c]	−25	−30	−47
	CH_3ONOH^+	49	52	54	
		50	52	55	
	$CH_3ON(H)=O^+$	48	50	50	
		48	50	50	
	$CH_3NO_2^{\bullet+} + H^\bullet$	488	488	503	
		487	487	502	500
	$CH_3^+ + HONO$	292	298	300	
		299	304	306	308
	$CH_3^\bullet + HONO^{+\bullet}$	423	415	435	
		430	422	442	
	$CH_3NO^{+\bullet} + OH^\bullet$	268	268	282	
		275	275	289	
	$CH_2NO^+ + H_2O$	61	48	51	
		69	55	59	
$CH_3O(H)-NO^+$	→ $CH_3OH + NO^+$	147	136	98	
(**2**$^+$)		149	137	99	125
	$CH_3ONO^{+\bullet} + H^\bullet$	459	460	473	
		461	463	475	495
$CH_3ON(H)=O^+$	→ $CH_3^+ + H-NO_2$	272	276	284	
(**3**$^+$)		278	282	291	
	$CH_3^\bullet + H-NO_2^{+\bullet}$	485	483	571	
		492	491	578	
	$CH_3O^\bullet + H-NO^{+\bullet}$	330	326	339	
		336	332	345	
CH_3ONOH^+	→ $CH_3O^\bullet + NOH^+$	389	390	403	
(**4**$^+$)		395	395	409	
$CH_3NO_2^{+\bullet}$	→ $CH_3^+ + NO_2^\bullet$	116	117	115	
		122	123	120	139
	$CH_3^\bullet + NO_2^+$	135	110	89	
		140	115	93	134
	$CH_3NO^{+\bullet} + (^3P)O$	208	212	194	
		212	216	198	
$CH_3NO_2^{+\bullet}$	→ $CH_3ONO^{+\bullet}$	−50	−57	−64	
		−50	−57	−64	−52
$CH_3ONO^{+\bullet}$	→ $CH_3O^\bullet + NO^+$	100	89	52	
		104	93	56	65
$HONO^{+\bullet}$	→ $NO^+ + OH^\bullet$	61	52	4	
		67	58	11	<47
$HONO^{+\bullet}$	→ $H^\bullet + NO_2^+$	201	182	156	
		205	187	160	<215
$H-NO_2^{+\bullet}$	→ $H^\bullet + NO_2^+$	90	64	−30	
		95	76	−26	

[a] In units of kJ mol^{-1}. [b] From reference 24. [c] 0 K energies in upper lines, 298 K energies in lower lines.

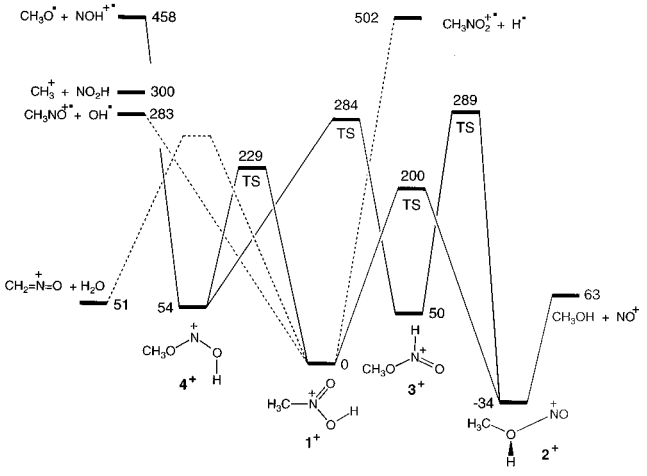

Figure 8. G2(PMP2) potential energy diagram for ion isomerizations and dissociations at 0 K in kJ mol^{-1}.

energy for the reverse addition of H$^\bullet$ was substantial, $E_a = 28$ kJ mol^{-1}. The path for the O−H bond dissociation was also investigated with UMP2(FULL)/6-31+G(d,p) calculations which found an earlier transition state at d(O−H) = 1.565 Å. The G2(PMP2) potential energy barrier at this TS was 200 kJ mol^{-1} giving the activation energy for the reverse H atom addition as 38.5 kJ mol^{-1}. The energy barriers for H atom addition had an effect on the reaction kinetics at the high-pressure limit as discussed below.

Cleavage of the C−N bond in **1** also required a barrier in a transition state (**TS2**) which was 116 kJ mol^{-1} above **1**. The reverse addition of $CH_3^\bullet$ to the nitrogen atom in nitrous acid had $E_a = 25$ kJ mol^{-1}. The reaction coordinate for the cleavage of the N−O bond was investigated up to 2.9 Å separation and showed continuously rising energy. Beyond 2.9 Å we encountered severe convergence problems with both UHF and B3LYP calculations. Although the presence of a small activation energy above the dissociation threshold (131 kJ mol^{-1} at 0 K) cannot be excluded completely from the present data, there is substantial evidence that OH$^\bullet$ additions are typically barrierless.[37] The radical relative and dissociation energies as calculated at various levels of theory are summarized in Table 4.

The potential energy diagram in Figure 10 also shows the Franck−Condon energies (E_{FC}) in vertical neutralization of **1**$^+$−

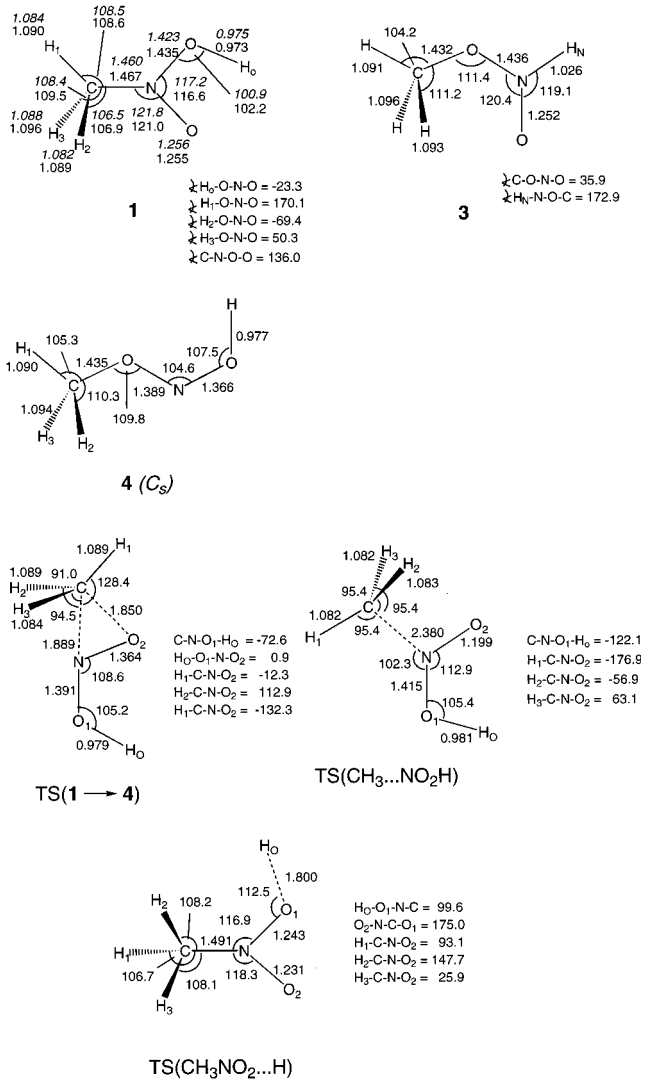

Figure 9. UB3LYP/6-31+G(d,p) optimized structures of **1**, **3**, **4**, and transition states. Bond lengths in angstroms, bond and dihedral angles in degrees. Roman numerals: B3LYP/6-31+G(d,p) optimized structures. Italic numerals: UMP2(FULL)/6-31+G(d,p) optimized structures.

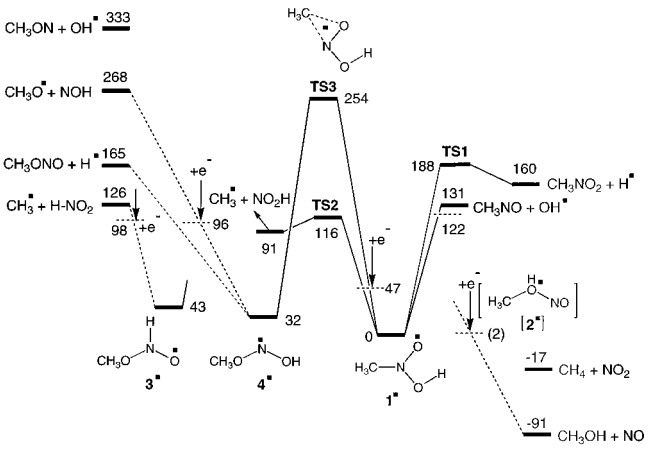

Figure 10. G2(PMP2) potential energy diagram for radical isomerizations and dissociations at 0 K in kJ mol^{-1}.

$\mathbf{4}^+$. The E_{FC} in **1** was moderate (47 kJ mol^{-1}) and alone insufficient to promote radical dissociation. The E_{FC} in **3** and **4** were also moderate (55 and 64 kJ mol^{-1}, respectively) and brought the vertically formed radicals close to the dissociation limits (Figure 10). Vertical neutralization of $\mathbf{2}^+$ formed an unbound radical whose energy was 93 kJ mol^{-1} above CH_3OH + NO (Figure 10).

Dissociation and Addition Kinetics. The calculated transition state energies were used for RRKM calculations of unimolecular rate constants for simple-bond dissociations in **1** at the low-pressure limit (Figure 11). As expected from the calculated activation energies, loss of H$^•$ by O−H bond cleavage was slower than the cleavages of the C−N and N−O bonds by several orders of magnitude at all relevant internal energies of **1**. In contrast, the latter two dissociations were competitive. The loss of methyl had a lower onset energy but a shallower log *k(E)* curve which crossed with that for loss of OH$^•$ at 142 kJ mol^{-1}. Hence, radicals **1** with internal energies below 142 kJ mol^{-1} will dissociate preferentially by loss of $CH_3^•$ to form HONO whereas a fraction with internal energies above 142 kJ mol^{-1} will form CH_3NO and OH$^•$. Note, however, that the slopes of the log *k(E)* curves for these two dissociations did not differ dramatically, so that both reactions can be expected to occur in competition over a relatively broad range of internal energies (Figure 11). The RRKM calculations were in good overall agreement with the NR spectra of **1** and the variable time measurements. Loss of H$^•$ from **1** was insignificant whereas the rate parameters for the formations of CH_3NO + OH$^•$ and $CH_3^•$ + HONO were very similar. It should be noted that the variable-time rate parameters average over a range of unimolecular rate constants and do not represent threshold-energy dissociations only.

The transition state energies were also used to calculate the thermal rate constants for hydrogen atom addition to nitromethane and dissociations of **1** at the high-pressure limit using standard transition-state theory (TST) formulas.[23] Both the H atom addition and dissociation showed linear Arrhenius plots ($r^2 = 0.999$) over a broad range of temperatures. The addition had $E_{Arrh} = 29.7$ kJ mol^{-1} and log $A = 12.84$, the dissociation had $E_{Arrh} = 193.1$ kJ mol^{-1} and log $A = 14.29$. The addition was fast even at 298 K, $k_{H,add} = 4.02 \times 10^7$ cm^3 mol^{-1} s^{-1}, whereas the loss of H was negligibly slow. However, the calculated rates of H-atom addition were lower than the experimental values measured in the 360−570 K range.[2a] This discrepancy originated from the different activation energies derived from the kinetic measurements ($E_a = 15.6$ kJ mol^{-1}) and G2(PMP2) calculations ($E_a = 27.1$ kJ mol^{-1}), while the log *A* terms were similar (12.67 and 12.84, respectively). The G2(PMP2) activation energy which was based on the MP2-(FULL) transition state showed even poorer agreement with experiment. It may be noted that the B3LYP/6-311+G(3df,2p) activation energy for the H atom addition (12 kJ mol^{-1}) gave, perhaps fortuitously, the best fit with the experiment although B3LYP overestimated the O−H bond dissociation energy in **1** by 19 kJ mol^{-1} (Table 3).

The rate constants for high-pressure dissociations of **1** by loss of H ($k_{H,diss}$), OH ($k_{OH,diss}$), and CH_3 ($k_{CH3,diss}$) are plotted in Figure 12. Relevant to hydrogen atom capture in flames, the data showed that if formed by H atom addition to nitromethane and thermalized by collisions, **1** will dissociate rapidly ($k \geq 10^4$ s^{-1}) to $CH_3^•$ + HONO and CH_3NO + OH$^•$ at temperatures above 600 K. The branching ratio for these two channels slightly favored formation of $CH_3^•$ + HONO below 1100 K, while the other dissociation should be faster above 1100 K. Both reactions are therefore predicted to occur in the range of temperatures characteristic for hydrocarbon flames.

Discussion

The ion and neutral energy data now allow us to discuss the formation and occurrence of dissociation products in the NR

TABLE 4: Radical Relative Stabilities and Dissociation Energies

reactant		products	energy[a] B3LYP/6-31+G(d,p)	B3LYP/6-311+G(3df,2p)	G2(PMP2)	exptl[b]
$CH_3NO_2H^\bullet$ (**1**)	→	$CH_3ONOH^\bullet$	38[c]	37	32	
			39[c]	38	34	
		$CH_3ON(H)-O^\bullet$	39	39	43	
			39	39	43	
		$CH_3NO_2 + H^\bullet$	189	181	160	
			194	186	165	
					162[d]	162
					167[d]	167
		TS(O···H)	198	193	188	
					200[d]	
		$CH_3NO + OH^\bullet$	144	143	131	
			150	149	136	
		TS(N···O)	(126)[e]	(128)	(122)	
		$CH_3^\bullet + NO_2H$	104	99	91	
			110	105	97	
		TS(C···N)	120	117	116	
		$CH_3OH + NO^\bullet$	−62	−71	−91	
			−57	−66	−87	
		$CH_4 + NO_2^\bullet$	−14	−22	−17	
			−8	−16	−12	
$CH_3ON(H)-O^\bullet$ (**3**)	→	$CH_3^\bullet + H-NO_2$	94	87	83	
			99	93	88	
		$CH_3O^\bullet + H-NO$	114	112	124	
			119	117	129	
$CH_3ONOH^\bullet$ (**4**)	→	$CH_3O^\bullet + NOH$	199	201	224	
			203	205	228	
		$CH_3ONO + H^\bullet$	161	155	133	
			165	159	137	
		$CH_3^\bullet + HONO$	67	61	59	
			71	66	63	
CH_3NO_2	→	$CH_3^\bullet + NO_2^\bullet$	228	224	247	
			234	230	254	254
		$CH_3NO + (^3P)O$	382	394	384	
			388	399	389	394
		CH_3ONO	10	11	5	
			10	11	5	8
CH_3ONO	→	$CH_3O^\bullet + NO^\bullet$	152	151	170	
			157	156	175	173
NO_2H	→	$NO^\bullet + OH^\bullet$	191	192	206	
			198	198	210	210

[a] In units of kJ mol^{-1}. [b] From reference 24. [c] 0 K energies in upper lines, 298 K energies in lower lines. [d] G2(PMP2) relative energies using UMP2(FULL)/6-31+G(d,p) optimized geometries and ZPVE corrections. [e] Energies at the kinetic bottleneck.

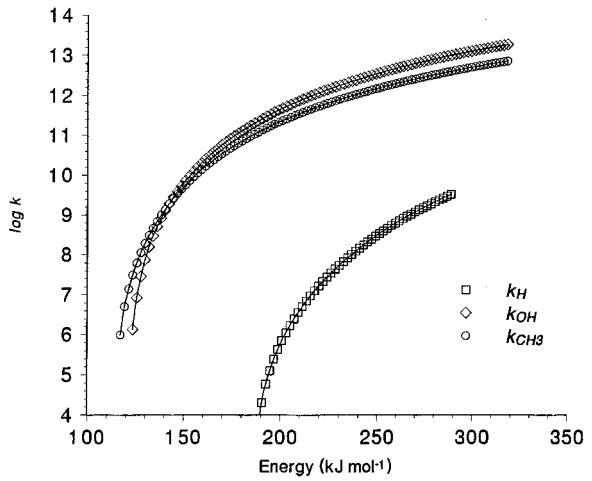

Figure 11. RRKM unimolecular rate constants for dissociations of **1** at the low-pressure limit. Squares: dissociation of the O−H bond: Diamonds: dissociation of the N−O bond. Circles: dissociation of the C−N bond.

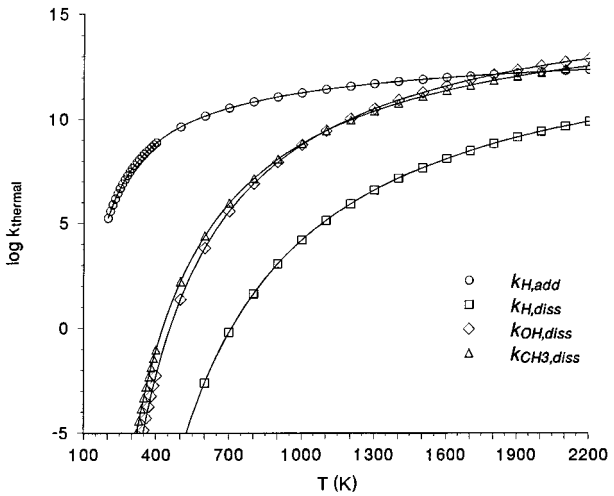

Figure 12. Addition and dissociation rate constants from TST calculations at the high-pressure limit. Circles: addition of H atom. Squares: dissociation of the O−H bond. Diamonds: dissociation of the N−O bond. Triangles: dissociation of the C−N bond.

mass spectra. The nitromethane molecule and cation-radical are both substantially stable to be detected if formed by neutral or ion dissociations (Tables 3 and 4).[28] In addition, the Franck−Condon energy in vertical ionization of nitromethane (34 kJ mol^{-1}) is insufficient to drive ion dissociations (Table 3). Hence

the absence of $CH_3NO_2^{+\bullet}$ in the NR spectrum of $\mathbf{1}^+$ means unambiguously that loss of H did not occur from **1** or $\mathbf{1}^+$. The dissociation of **1** to HONO and $CH_3^\bullet$ did not give rise to an abundant peak of reionized $HONO^{+\bullet}$. Table 3 shows that $HONO^{+\bullet}$ was only weakly bound toward dissociation to NO^+ and $OH^\bullet$. In addition, vertical ionization of HONO was accompanied by 50 kJ mol^{-1} Franck−Condon energy which was sufficient to promote ion dissociation. Remarkably, NR of $HONO^{+\bullet}$ prepared by protonation of NO_2 yielded a weak survivor ion. This could not be due to an isomer, $H-NO_2^{+\bullet}$, which was substantially less stable than $HONO^{+\bullet}$ and metastable with regard to dissociation to NO_2^+ and $H^\bullet$ (Table 3). The small fraction of survivor $HONO^{+\bullet}$ can be attributed to reionization of vibrationally hot HONO in which the Franck−Condon energy was diminished by an improved geometry match between the higher vibrational states of HONO and the ground vibrational state of $HONO^{+\bullet}$.[38]

The methyl nitrite cation-radical was weakly bound toward the lowest-energy dissociation to $CH_3O^\bullet$ and NO^+ (Table 3). The dissociation energy can be almost entirely supplied by Franck−Condon effects in vertical ionization (55 kJ mol^{-1}). It should be noted, however, that methyl nitrite gives a 15−20% fraction of stable molecular ions upon electron ionization, while the Xe/O_2[28] and CH_3SSCH_3/O_2 NR spectra of $CH_3ONO^{+\bullet}$ did not yield a detectable survivor ion. Hence, the absence of a $[C,H_3,N,O_2]^{+\bullet}$ peak corresponding to CH_3ONO in the NR spectrum of $\mathbf{2}^+$ alone did not exclude that a fraction of **2** dissociated by loss of H. However, there is no doubt from both experiment and theory that the major dissociation of **2** proceeded to form CH_3OH and NO.

The less stable isomers $\mathbf{3}^+$ and $\mathbf{4}^+$ were formed by highly exothermic protonation of methyl nitrite but were not distinguished by the NR spectra. Table 3 shows that both $\mathbf{3}^+$ and $\mathbf{4}^+$ required high energies for bond dissociations and >200 kJ mol^{-1} potential energy barriers to isomerizations (Figure 8). Such energies could be supplied by neither the protonation exothermicities[39] nor Franck−Condon effects on vertical ionization which were 116 and 73 kJ mol^{-1} for **3** and **4**, respectively. By contrast, the protonation exothermicity in the formation of $\mathbf{2}^+$, $\Delta H_r = PA(CH_3)\mathbf{O}\text{-}NO) - PA(CH_4) = 261$ kJ mol^{-1}, even when scaled by ~80% energy partitioning into the ion,[40] exceeded greatly the dissociation energy of the O−N bond in $\mathbf{2}^+$ and should cause very rapid ion dissociation of an estimated $k_{uni} > 10^{12}$ s^{-1}. It is therefore likely that the *stable* ion population that were sampled for collisional neutralization did not contain $\mathbf{2}^+$ and consisted mainly of $\mathbf{3}^+$ and $\mathbf{4}^+$.

The neutral isomers **3** and **4** differed in the dissociation energies of the $O-CH_3$ bonds, which was more facile in **4** (Table 4). In addition, the Franck−Condon energy in vertical neutralization of $\mathbf{3}^+$ and $\mathbf{4}^+$ (55 and 64 kJ mol^{-1}, respectively) exceeded the C−O bond dissociation energy in **4** but not in **3**. Hence it can be concluded that vertically formed **4** dissociated while **3** did not, so that the survivor ion observed in the NR mass spectrum of the mixture must belong to $\mathbf{3}^+$. In contrast to the loss of methyl from **1**, those from **3** and/or **4** gave rise to a detectable peak of $H-NO_2^{+\bullet}$ and/or $HONO^{+\bullet}$, respectively. This can be explained as follows. From the protonation/neutralization energetics for the formation of $\mathbf{3}^+$, **3**, $\mathbf{4}^+$, and **4**, it can be inferred that fractions of the radicals were formed with up to 200 kJ mol^{-1} internal energy.[39] Dissociation by methyl loss of these hot radicals formed HONO and/or HNO_2 with up to 120−140 kJ mol^{-1} internal energy which resulted in significant population of excited vibrational states. Vertical ionization of these can produce a fraction of stable $HONO^{+\bullet}$ as discussed above. It should be noted that the observation of both survivor $\mathbf{3}^+$ and $HONO^{+\bullet}$ indicated that the intermediate radicals **3** and **4** were formed with a wide range of internal energies, as expected from the combination of exothermic protonation and Franck−Condon effects.[25a]

Similar arguments can be used to discuss the dissociations of **1**. The upper bound for the internal energy in vertically formed ground electronic state of **1** was estimated at 225 kJ mol^{-1} from a combination of nitromethane thermal energy (15 kJ mol^{-1} at 523 K), 80% of the protonation exothermicity deposited in the ion[40] (169 kJ mol^{-1}) and the Franck−Condon energy in vertical neutralization of $\mathbf{1}^+$ (47 kJ mol^{-1}). This exceeded the dissociation thresholds for the C−N and N−O bond cleavages, but not the barrier for isomerization to **4** (Figure 10). The log *k(E)* curves in Figure 11 showed that the O−H bond cleavage was not competitive in **1** even at the above internal energy limit. The branching ratio for the formations of $CH_3NO + OH^\bullet$ and $CH_3^\bullet + HONO$ depended on the internal energy distribution in the dissociating **1** (Figure 11).

Conclusions

Radical **1** corresponding to the hydrogen atom adduct to nitromethane was prepared for the first time in the gas phase and characterized by neutralization−reionization mass spectrometry and ab initio calculations. Radical **1** was stable on the μs time scale. The dominant unimolecular dissociations were cleavages of the C−N and N−O bonds that were distinguished by variable-time measurements. The unimolecular chemistry of **1** can be explained by the properties of the ground electronic state. The hydrogen atom adducts to methyl nitrite differed in their stabilities. Hydrogen atom addition to the inner oxygen atom was predicted to produce an unbound species (**2**). In keeping with the theoretical prediction, radical **2** formed by collisional neutralization of its cation dissociated without a barrier to methanol and nitrogen oxide. Hydrogen atom addition to the nitrogen and terminal oxygen atoms in methyl nitrite was predicted to produce stable radicals **3** and **4**, respectively. Radical **3** was detected following neutralization of a cation mixture and reionization. Radical **4** was predicted to dissociate due to a combination of ion internal energy and Franck−Condon energy upon collisional neutralization.

Acknowledgment. Support of this work by a grant from the National Science Foundation (CHE-9712750) is gratefully acknowledged. Computational support was provided by the Department of Chemistry Computer Cluster that received generous funding from NSF (Grant CHE-9808182) and University of Washington.

Supporting Information Available: Tables 1S and 2S of B3LYP/6-31+G(d,p), B3LYP/6-311+G(3df,2p) and G2(PMP2) total energies, zero-point, and enthalpy corrections for relevant ions and neutral species. This information is available free of charge via the Internet at http://pubs.acs.org.

References and Notes

(1) For reviews see, for example: (a) Gardiner, W. C., Jr., Ed. *Combustion Chemistry*, Springer-Verlag: New York, 1984. (b) Egsgaard, H. *Ion Chemistry of the Flame*; Risø National Laboratory: Roskilde, Denmark, 1993.

(2) (a) Ko, T.; Flaherty, F.; Fontijn, A. *J. Phys. Chem.* **1991**, *95*, 6967. (b) Slemr, F.; Warneck, P. *Ber. Bunsen-Ges. Phys. Chem.* **1975**, *79*, 1163. (c) Salter, L. F.; Thrush, B. A. *J. Chem. Soc., Faraday Trans. 1*, **1977**, 2025. (d) Nielsen, O. J.; Sidebottom, H. W.; O'Farell, D. J.; Donlon, M.; Treacy, J. *Chem. Phys. Lett.* **1988**, *146*, 197.

(3) Thomsen, E. L.; Nielsen, O. J.; Egsgaard, H. *Chem. Phys. Lett.* **1993**, *215*,. 257.

(4) For an earlier theoretical study of $[C,H_4,N,O_2]$ radicals, see: Melius, C. P. *J. Phys. Colloid. C4* **1987**, *48*, 341.

(5) For reviews of the technique, see: (a) Wesdemiotis, C.; McLafferty, F. W. *Chem. Rev.* **1987**, *87*, 485. (b) Terlouw, J. K.; Schwarz, H. *Angew. Chem., Int. Ed. Engl.* **1987**, *26*, 805. (c) Holmes, J. L. *Mass Spectrom. Rev.* **1989**, *8*, 513. (d) Terlouw, J. K. *Adv. Mass Spectrom.* **1989**, *11*, 984. (e) McLafferty, F. W. *Science*, **1990**, *247*, 925. (f) Turecek, F. *Org. Mass Spectrom.* **1992**, *27*, 1087. (g) Goldberg, N.; Schwarz, H. *Acc. Chem. Res.* **1994**, *27*, 347. (h) Schalley, C. A.; Hornung, G.; Schroder, D.; Schwarz, H. *Chem. Soc. Rev.* **1998**, *27*, 91. (i) Turecek, F. *J. Mass Spectrom.* **1998**, *33*, 779.

(6) (a) Kuhns, D. W.; Tran, T. B.; Shaffer, S. A.; Turecek, F. *J. Phys. Chem.* **1994**, *98*, 4845. (b) Kuhns D. W.; Turecek, F. *Org. Mass Spectrom.* **1994**, *29*, 463.

(7) (a) Sadilek, M.; Turecek, F. *Chem. Phys. Lett.* **1996**, *263*, 203. (b) Sadilek, M.; Turecek, F. *J. Phys. Chem.* **1996**, *100*, 9610. (c) Nguyen, V. Q.; Sadilek, M.; Frank, A. J.; Ferrier, J. G.; Turecek, F. *J. Phys. Chem. A*, **1997**, *101*, 3789.

(8) (a) Curtiss, L. A.; Raghavachari, K.; Pople, J. A. *J. Chem. Phys.* **1993**, *98*, 1293. (b) Curtiss, L. A.; Raghavachari, K.; Redfern, P. C.; Pople, J. A. *J. Chem. Phys.* **1997**, *106*, 1063. (c) Raghavachari, K.; Stefanov, B. B.; Curtiss, L. A. *J. Chem. Phys.* **1997**, *106*, 6764.

(9) (a) Robinson, P. J.; Holbrook, K. A. *Unimolecular Reactions*; Wiley-Interscience: New York, 1972. (b) Gilbert, R. G.; Smith, S. C. *Theory of Unimolecular and Recombination Reactions*; Blackwell: London, 1990.

(10) Turecek, F.; Gu, M.; Shaffer, S. A. *J. Am. Soc. Mass Spectrom.* **1992**, *3*, 493.

(11) Gilman, J. P.; Hsieh, T. and Meisels, G. G. *J. Chem. Phys.* **1983**, *78*, 1174.

(12) Frisch, M. J.; Trucks, G. W.; Schlegel, H. B.; Gill, P. M. W.; Johnson, B. G.; Robb, M. A.; Cheeseman, J. R.; Keith, T. A.; Petersson, G. A.; Montgomery, J. A.; Raghavachari, K.; Al-Laham, M. A.; Zakrzewski, V. G.; Ortiz, J. V.; Foresman, J. B.; Cioslowski, J.; Stefanov, B. B.; Nanayakkara, A.; Challacombe, M.; Peng, C. Y.; Ayala, P. Y.; Chen, W.; Wong, M. W.; Andres, J. L.; Replogle, E. S.; Gomperts, R.; Martin, R. L.; Fox, D. J.; Binkley, J. S.; Defrees, D. J.; Baker, J.; Stewart, J. P.; Head-Gordon, M.; Gonzalez, C.; Pople, J. A. *Gaussian 94* (Revision D.1); *Gaussian*, Inc.: Pittsburgh, PA, 1995.

(13) Becke, A. D. *J. Chem. Phys.* **1993**, *98*, 1372, 5648. (b) Stephens, P. J.; Devlin, F. J.; Chablowski, C. F.; Frisch, M. J. *J. Phys. Chem.* **1994**, *98*, 11623.

(14) Møller, C.; Plesset, M. S. *Phys. Rev.* **1934**, *46*, 618.

(15) Turecek, F.; Cramer, C. J. *J. Am. Chem. Soc.* **1995**, *117*, 12243.

(16) See for example: (a) Bauschlicher, C. W.; Partridge, H. *J. Chem. Phys.* **1995**, *103*, 1788. (b) Frank, A. J.; Sadilek, M.; Ferrier, J. G.; Turecek, F. *J. Am. Chem. Soc.* **1996**, *118*, 11321. (c) Frank, A. J.; Sadilek, M.; Ferrier, J. G.; Turecek, F. *J. Am. Chem. Soc.* **1997**, *119*, 12343. (d) Turecek, F. *J. Phys. Chem. A*, **1998**, *102*, 4703.

(17) Schlegel, H. B. *J. Chem. Phys.* **1986**, *84*, 4530.

(18) Wong, M. W. *Chem. Phys. Lett.* **1996**, *256*, 391.

(19) (a) Rauhut, G.; Pulay, R. *J. Phys. Chem.* **1995**, *99*, 3093. (b) Finley, J. W.; Stephens, P. J. *J. Mol. Struct. (THEOCHEM)* **1995**, *357*, 225. (c) Scott, A. P.; Radom, L. *J. Phys. Chem.* **1996**, *100*, 16502.

(20) Pople, J. A.; Head-Gordon, M.; Raghavachari, K. *J. Chem. Phys.* **1987**, *87*, 5968.

(21) Zhu, L.; Hase, W. L. *Quantum Chemistry Program Exchange*; Indiana University; Bloomington, IN, 1994; Program No. QCPE 644.

(22) Zhu, L.; Hase, W. L. *Chem. Phys. Lett.* **1990**, *175*, 117.

(23) Levine, I. N. *Physical Chemistry*, 3rd ed.; McGraw-Hill: New York, 1988; pp. 839−841.

(24) Mallard, W. G.; Linstrom, P. J.; Eds. NIST Chemistry Webbook, NIST Standard Reference Database No. 69; National Institute of Standards and Technology: Gaithersburg, MD, March 1998. http//webbook.nist.gov/chemistry.

(25) (a) Nguyen, V. Q.; Turecek, F. *J. Mass Spectrom.* **1996**, *31*, 843. (b) Nguyen, V. Q.; Turecek, F. *J. Am. Chem. Soc.* **1997**, *119*, 2280.

(26) Polasek, M.; Turecek, F. *Int. J. Mass Spectrom.* **1999**. In press.

(27) Pagsberg, P.; Ratajczak, E.; Sillesen, A.; Latajka, Z. *Chem. Phys. Lett.* **1994**, *227*, 6.

(28) Egsgaard, H.; Carlsen, L.; Florencio, H.; Drewello, T.; Schwarz, H. *Ber. Bunsen-Ges. Phys. Chem.* **1989**, *93*, 76.

(29) Fitch, W. L.; Sauter, A. D. *Anal. Chem.* **1983**, *55*, 832.

(30) Sadilek, M.; Turecek, F. *J. Phys. Chem.* **1996**, *100*, 224.

(31) Bartmess, J. E.; Georgiadis, R. M. *Vacuum*, **1983**, *33*, 149.

(32) Summers, R. L. *NASA Technical Note TN D-5285*; National Aeronautics and Space Administration: Washington, DC, June 1969.

(33) Aschi, M.; Grandinetti, F. *Chem. Phys. Lett.* **1996**, *258*, 123.

(34) Lias, S. G.; Liebman, J. F.; Levin, R. D. *J. Phys. Chem. Ref. Data* **1984**, *13*, 695.

(35) Farid, R.; McMahon, T. B. *Int. J. Mass Spectrom. Ion Phys.* **1978**, *27*, 163.

(36) (a) Williams, D. H. *Acc. Chem. Res.* **1977**, *10*, 280. (b) McLafferty, F. W.; Turecek, F. *Interpretation of Mass Spectra*, 4th ed.; University Science Books: Mill Valley, CA, 1993; Chapter 7, pp 130−132.

(37) Atkinson, R. *Gas-Phase Tropospheric Chemistry*, *Journal of Physical Chemistry Reference Data Monograph No. 2*; American Institute of Physics: Woodbury, NY, 1994.

(38) Nguyen, V. Q.; Shaffer, S. A.; Turecek, F.; Hop, C. E. C. A. *J. Phys. Chem.* **1995**, *99*, 15454.

(39) From the protonation exothermicity, $-\Delta H_r = PA(CH_3O\mathbf{N}{=}O) - PA(CH_4) = 159$ kJ mol^{-1}, 80% partitioned in the ion,[40] vibrational thermal energy of CH_3ONO at the ion source temperature (15 kJ mol^{-1} at 250 °C), and Franck−Condon energy in vertical neutralization (55 kJ mol^{-1}), E_{int}(**3**) $= 159 \times 0.8 + 15 + 55 = 197$ kJ mol^{-1}.

(40) Uggerud, E. *Adv. Mass spectrom.* **1995**, *13*, 53.